 doi:10.20944/preprints201807.0582.v1

Article

ZnO nanoparticles anchored on a N-doped graphene-coated separator for a high performance lithium/sulfur battery

Suyu Wang[1], Fan Gao[1], Ruina Ma[1], An Du[1], Taizhe Tan[2], Miao Du[3], Xue Zhao[1*], Yongzhe Fan[1*], Ming Wen[1]

1 School of Materials Science and Engineering, Hebei University of Technology, 29 Guangrong Road, Tianjin 300130, PR China.

2 Synergy Innovation Institute of GDUT, Heyuan, Guangdong Province, China.

3 School of Chemistry and Chemical Engineering, Qilu Normal University, Jinan, 250200, China

* Corresponding author: zhaoxue@hebut.edu.cn, fyz@hebut.edu.cn

Tel.: +86-18892299872 +86-13512923308

Abstract: Fabrication of a nanocrystal zinc oxide (ZnO)/nitrogen-doped (N-doped) graphene composite using a novel and facile in situ sol-gel technique is demonstrated. Two-dimensional nanostructure morphology with uniform ZnO nanoparticles (average diameter of 10.25 nm) anchored on N-doped graphene nanosheets was observed via electron microscopy. Because of the polar heteroatoms on the graphene sheets, an abundance sites for polysulfide absorption were provided. More importantly, the strong chemical interaction between ZnO and polysulfides efficiently hindered the transport of polysulfides. Consequently, the lithium/sulfur (Li/S) battery with the ZnO/N-doped graphene composite-coated separator delivered enhanced performance in terms of discharge capacity and cycling stability when compared to the cell with a normal separator. With the modified separator, the battery achieved a discharge capacity as high as 942 mAh g^{-1} for the first cycle and remained at 90.02 mAh g^{-1} after the 100th charge/discharge test at 0.1 C. Results indicate that impeding the shuttling of polysulfides contributes to efficiently improving the behavior of the Li/S battery.

Keywords: ZnO/N-doped graphene composite; modified separator; lithium/sulfur batteries.

1. Introduction

With the fast development of the portable electronics sector, lithium/sulfur (Li/S) batteries are now being considering a promising candidate for energy storage systems because of their green transportation and high capacity. The Li/S battery has a theoretical energy density that is 5 times as large as that of a Li-ion battery [1,2]. Despite significant advances, various problems limit the widespread commercial application of Li/S batteries, including rapid capacity decline, low charge/discharge efficiency, and short cycle life, which are mainly caused by the soluble intermediate lithium polysulfides (LiPs) (Li_2S_n $4 \le n \le 8$) and their diffusion into the lithium metal anode (i.e., the proverbial "shuttle effects") [3-6]. More unfortunately, dissolved LiPs are ultimately reduced to insulating products (Li_2S/Li_2S_2), passivate the counter electrode, and deteriorate the rate performance of Li/S batteries.

The separator is a critical component in the battery; it enables ionic flow but prevents an internal short-circuit [7]. Dissolved LiPs necessarily diffuse through the membranes during electrochemical processes in the cell, and therefore, a variety of approaches to modify the separator have been explored to improve conductivity and impede LiP shuttling. Carbon materials, such as carbon black [8], graphene [9], reduced graphene (RGO) [10,11], multiwall carbon nanotubes (MWCNTs) [12], and microporous carbon paper [13] have been developed as sulfur hosts because of their abundant advantages: (1) their large specific surface area and intricate web structure, which contribute to physical LiP trapping; (2) their excellent electrical conductivity, which acts as an

 doi:10.20944/preprints201807.0582.v1

"upper current" collector to reuse the LiPs as a consequence and compensate for the rapid capacity decline; (3) their flexible mechanical strength, which accommodates volume changes. Zhu [14] et al. coated carbon on a separator and achieved marked cycle life with a capacity of 956 mAh g^{-1} after the 200th charge/discharge test and excellent rate performance of the Li/S battery. In further research, Zhang [3] et al. coated a functional layer of conductive carbon on the separator, and the cell delivered a noted retention ratio of 72.71% after the 100th cycling test at 0.5 C, which suggests that this approach alleviates the shuttling of LiPs. Also, it is worth mentioning that various metal oxides have been employed to modify separators because of their strong chemical bonding with migrating LiPs. To date, many metal oxides (such as $Mg_{0.6}Ni_{0.4}O$ [15], TiO_2 [16-18], Al_2O_3 [19,20], SnO_2 [21], MgO [22], and $NiFe_2O_4$ [23]) have shown an ability to suppress the shuttling of LiPs, resulting in decreased capacity decline and better electrical performance of the Li/S battery. For example, Evers [5] et al. coated nanosized TiO_2 particles on the separator, and this increased the cycling performance of the Li/S battery [5]. Guo [24] et al. synthesized nanocrystal CeO_2 with abundant –OH and $–NO_2$, which are responsible for the enhanced electrochemical performance when CeO_2 is used as an additive in a sulfur composite in Li/S cells. Results confirmed that the additive can adsorb sulfur and LiPs during charge/discharge processes, and this suppresses the migration of LiPs in the electrolyte and leads to marked improvement in the cycling stability and utilization of the active material of the cell. Because it is abundant in nature, low cost, and environmentally friendly, ZnO is considered to be a promising candidate for modifying the separator. Kong [25] et al. synthesized a composite of carbon materials with nanoflake morphology and ZnO; the composite was coated on the separator and achieved a stable capacity of 927 mAh g^{-1} after the 100th cycling test at 0.1 C, and this was attributed to the high conductivity of carbon materials and to the chemical inhibition of LiPs. We were inspired by the study of Li [26] et al., which synthesized a ZnO/graphene nanocomposite via a simple in situ sol-gel method. Herein, our aim was to modify a traditional separator (Gelgard 2400) by preparing a membrane that combined the advantages of a carbon material (N-doped graphene) and a metal oxide (ZnO) via a simple and cheap in situ sol-gel technique.

2. Experimental

2.1. Material Preparation

N-doped graphene (NDG) was purchased from Nanjing Xianfeng Nanoparticles Technology Company. First, zinc acetate (2.86 g) and NDG (0.0085 g) were dispersed in ethanol (130 mL) and ultrasonicated for 1 h to form a homogeneous solution. Then, ethanol solution (130 mL) with LiOH (0.754 g) additive were added to the above solution, which was magnetically stirred at 25 ℃ for 15 days; a black suspension was obtained. After washing several times with deionized (DI) water and ethanol, the collected products were placed in a vacuum oven at 50 ℃ overnight.

2.2. Characterization

The crystal structure of the as-prepared ZnO/NDG composite was investigated using an X-ray diffractometer (XRD, Vinci, AXS) equipped with Cu-Kα radiation. Elemental analysis was conducted using an X-ray spectrometer (XPS, ESCALAB250Xi). Morphologies and detailed structures of the samples were observed using a scanning electron microscope (SEM, NovaNano SEM450, FEI) and transmission electron microscope (TEM, JEM2010F). Chemical transformation of the composite was determined using Fourier transform infrared (FTIR) spectroscopy. Raman spectra were obtained using a Raman spectroscope (LabRAM HR Evolution, HORIBA).

2.3. Electrochemical Measurements

Preparation of the cathode material was illustrated in a study by Yin [27] et al. The cathode material with carbon black and polyvinylidene fluoride (PVDF) binder (8:1:1 by weight) were mixed in N-methyl-2-pyrrolidone (NMP) to form a slurry that was coated on Al foil. After drying at 60 ℃ for 6 h, the Al foil was cut into circles (diameter of 10 mm) to prepare the positive electrodes. To make a modified separator, a slurry of the as-prepared ZnO/NDG composite and PVDF binder (6:4

Preprints (www.preprints.org) | NOT PEER-REVIEWED | Posted: 30 July 2018 doi:10.20944/preprints201807.0582.v1

by weight) in NMP were coated onto a commercial separator (Gelgard 2400) and dried at 50 ℃ in a vacuum oven overnight. CR 2025 coin cells were assembled inside a glove box filled with argon (99.9995 % Ar); lithium metal foil served as the anode, and 1 M lithium trifluoromethanesulfony imide (LiTFSI) in a mixed solvent of 1,3-dioxolane (DOL) and 1,2-dimethoxyethane (DME) (1:1 by volume) served as the electrolyte. Charge/discharge tests were conducted between 1.7-2.8 V at various current densities (C) using a multichannel battery tester (BT-2000, Arbin).

3. Results and Discussion

A schematic diagram of the Li/S cell configurations with and without the modified separator during the cycling process is illustrated in Fig. 1a. Compared to the routine separator, which has an abundance of large pores (several micrometers) and failed to impede the shuttling of polysulfides (1-8 nm), the modified separator coated with the ZnO/NDG composite can efficiently suppress such shuttling. A schematic diagram of the ZnO/NDG composite structure and functional mechanism is shown in Fig. 1b; the ZnO nanoparticles that are anchored onto the NDG sheets mitigate restacking of the graphene sheets and also chemically restrict the diffusion of polysulfides.

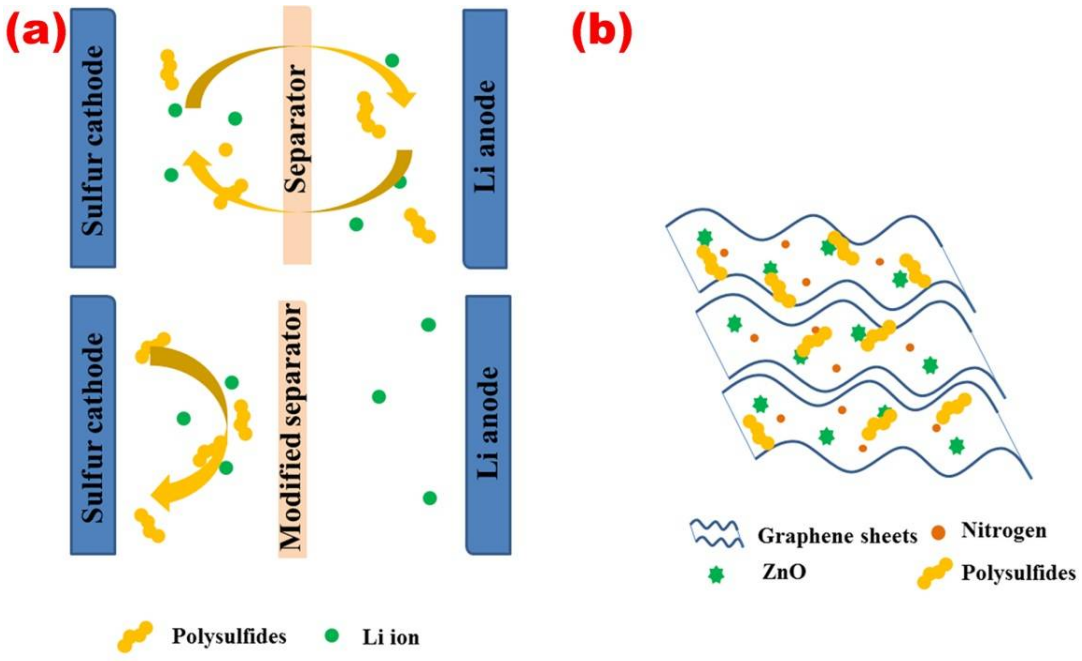

Fig. 1. Schematic diagram of the cell configuration with a normal separator (top) and with the ZnO/N-doped composite-coated separator (bottom) (a). Functional mechanism of the ZnO/N-doped composite-coated separator (b).

Fig. 2a shows the XRD patterns of pure ZnO, NDG, and the ZnO/NDG composite. Broad diffraction peaks observed at 26.3° and 43.3° can be respectively ascribed to the (022) and (100) crystalline lattice planes of NDG. Peaks at 31.8°, 34.4°, 36.2°, 47.5°, 56.6°, 62.9°, 68.0°, and 69.1° correspond respectively to the (100), (002), (101), (102), (110), (103), (112), and (201) crystalline lattice planes of the hexagonal structure of ZnO (JCPDS 36-1451). Note that these peaks in the ZnO/NDG composite are relatively broad, which suggests that the ZnO particles are nanosize. The Raman spectrum is shown in Fig. 2b; the calculated intensity ratio of the D and G bands (I_D/I_G) is an indication of whether the structure of the graphene sheets is disordered or not. The values of I_D/I_G were calculated to be 1.054 and 1.010 for the ZnO/NDG composite and NDG, respectively, and these values suggest that ZnO nanoparticles were introduced onto the surface of the NDG nanosheets. To investigate the chemical compositio of ZnO/NDG composite, XPS was conducted. Fig. 2c shows the high-resolution XPS N 1s spectra. Peaks centered 398.1 eV and 398.5 eV can be assigned to pyridinic-type N (a N atom that replaces a C atom in a hexagon) [28]. The peak at 399.2 eV is

Preprints (www.preprints.org) | NOT PEER-REVIEWED | Posted: 30 July 2018 doi:10.20944/preprints201807.0582.v1

associated with ionized pyridine N [28]. Peaks at 399.9 eV and 400.6 eV correspond to pyrrolic N (a nitrogen atom in a five-membered ring). The peak at 401.1 eV is attributed to graphitic N. From the Zn 2p spectrum (Fig. 2d), the peak with binding energy at 1021.9 eV is assigned to ZnO 2p 3/2, and peaks at 1044.7 eV and 1045.5 eV are indexed to ZnO 2p 1/2. All of these results indicate that the 2D ZnO/NDG composite interaction architecture was successfully fabricated using the simple in situ sol-gel technique. Interestingly, when comparing Fig. 2d with Fig. 2e, it can be seen that the peak at 1021.9 eV (ZnO 2p 3/2) before cycling was split into two peaks at 1021.9 eV (ZnSO4 2p 3/2) and 1022.0 eV (ZnS 2p 3/2) after cycling; this confirms the chemical interaction between ZnO and LiPs. Peaks located at 1044.7 eV and 1045.5 eV before cycling were negatively shifted to 1044.7 eV and 1045.5 eV, respectively, after cycling, and this corresponds to the absorption of sulfur-related species by the Zn-O bonding. In the S 2p spectrum after cycling (Fig. 2f), the peak centered at 168.3 eV can be assigned to sulfate, and the peaks at 169.0 eV, 169.9 eV, and 170.7 eV are related to metal-SO_4^{2-} species, which is in good accordance with the results of the Zn 2p spectrum after cycling.

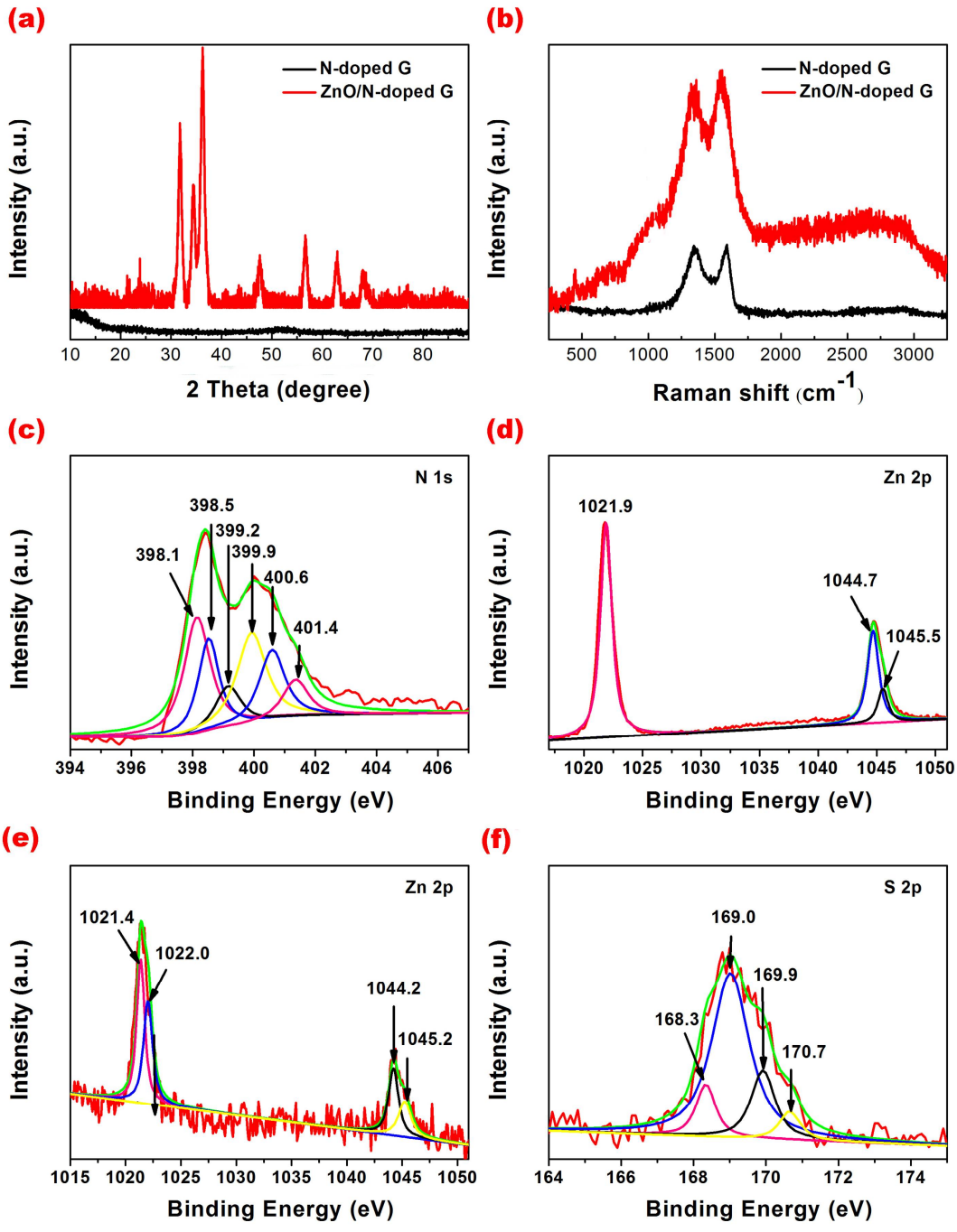

Preprints (www.preprints.org) | NOT PEER-REVIEWED | Posted: 30 July 2018 doi:10.20944/preprints201807.0582.v1

Fig. 2. XRD patterns of NDG and the ZnO/NDG composite (a). Raman spectra of NDG and the ZnO/NDG composite (b). XPS spectra of N 1s (c) and Zn 2p (d). XPS spectra of Zn 2p (e) and S 2p (f) after cycling.

SEM and TEM images of the sample are shown in Fig. 3. As seen in Fig. 3a, the porous NDG nanosheets were formed and coated with nanosized ZnO particles. The TEM images (Fig. 3b) further confirmed that the ZnO nanoparticles in the as-prepared ZnO/NDG composite were uniformly dispersed on the NDG sheets; the sizes of the ZnO particles ranged from 5 nm to 14 nm, as seen in Fig. 3c. The inset in Fig. 3c shows the particle diameter distribution of ZnO obtained from the TEM data, and the ZnO particles have a uniform size distribution with an average diameter of 10.25 nm. As seen in the high-resolution TEM image (Fig. 3d), lattice fringes of ZnO were clearly observed with an interlayer distance of the (101) plane (0.248 nm). It is worth noting that nanosized ZnO particles create shorter pathways for Li^+, and this contributes to improvements in the C rate performance of the cell.

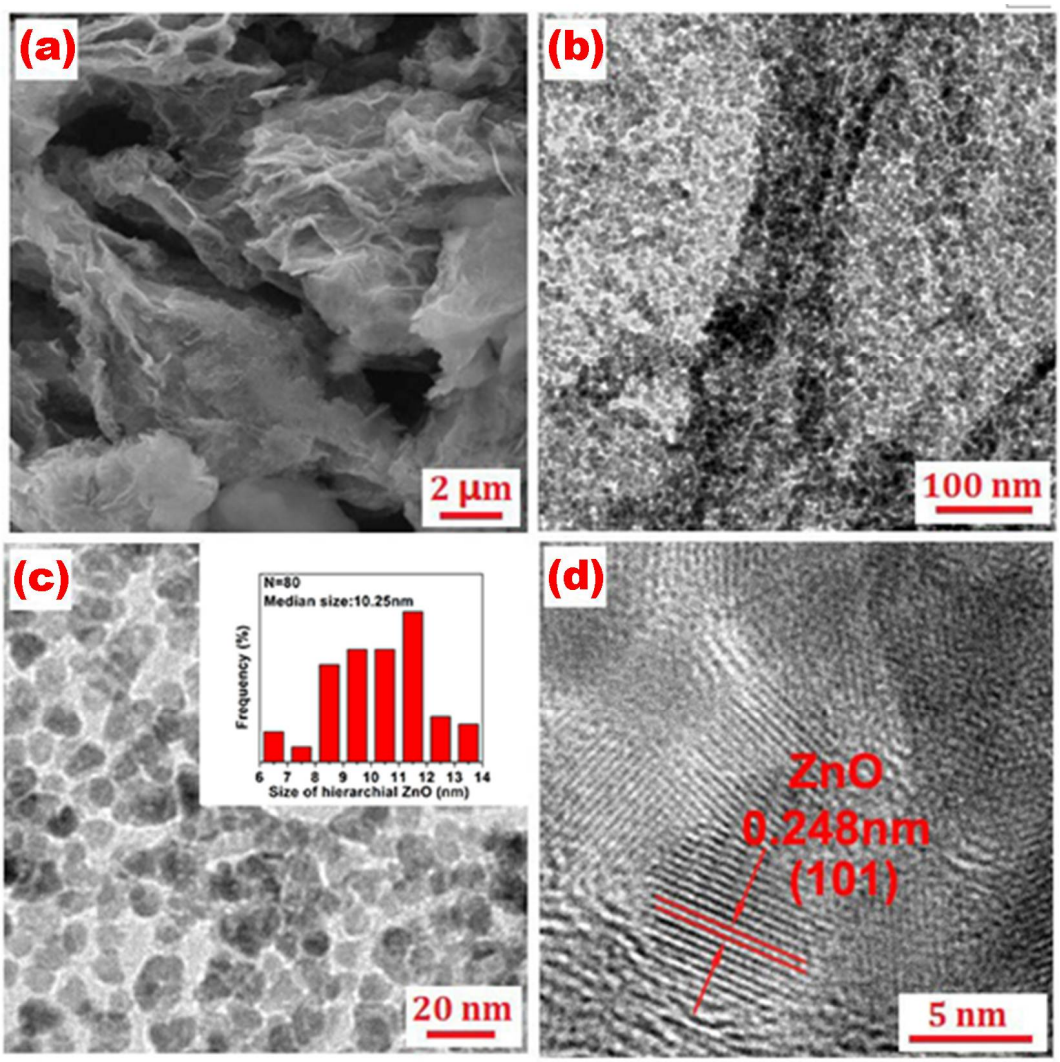

Fig. 3. SEM image of the ZnO/NDG composite (a). TEM image of the ZnO/NDG composite (b). Low-magnification TEM image for ZnO/NDG composite (c). HRTEM image of the ZnO/NDG composite (d). Distribution of ZnO particle size (inset of (c)).

Fig. 4a shows a top-view SEM image of a traditional commercial separator, which has an abundance of pores that are several micrometers in size, and these make it difficult for the separator to block the shuttling of LiPs (1-1.8 nm). Fig. 4b shows a typical front-view SEM image of the ZnO/NDG composite-coated separator. In contrast to the commercial separator, a rough surface forms a perfect blanket covering over the pores of the normal separator; this also provides a larger

 doi:10.20944/preprints201807.0582.v1

contact area with the electrolyte and contributes to suppressing the charge transfer resistance. The cross-section view of the modified separator in the inset of Fig. 4b displays a uniform coating layer with a thickness of around 25 μm.

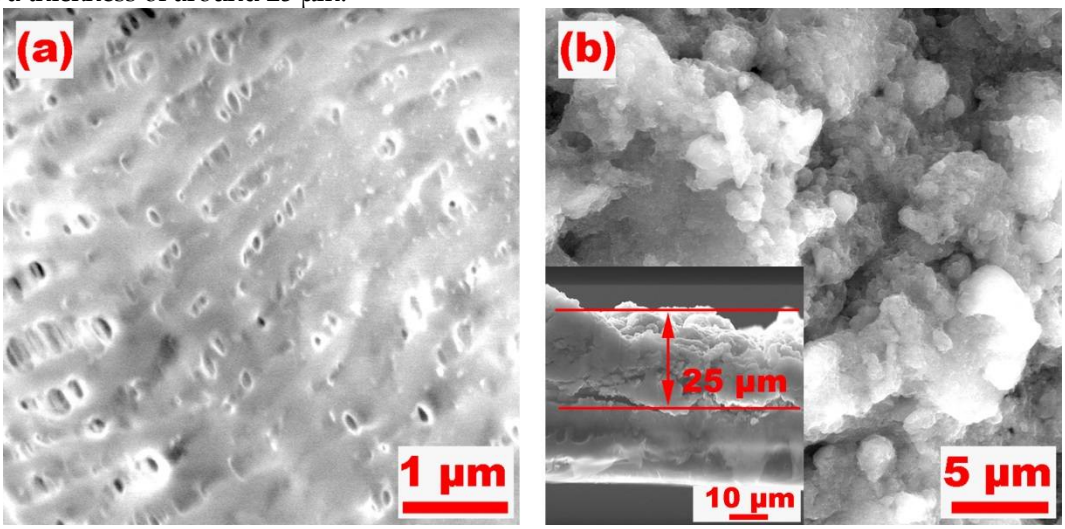

Fig. 4. Top-view SEM images of a normal separator (a) and the ZnO/NDG composite-coated separator (b). Cross-section view of the modified separator (inset in (b)).

Fig. 5a depicts profiles of the typical first three cycles of the charge/discharge processes of the cell with the ZnO/NDG composite-coated separator at a rate of 0.1 C; two-step redox reaction features are revealed. Plateaus at 2.4 V and 2.1 V were indexed to the oxidation of S_8 to LiPs and the reduction of the LiPs to sulfides, respectively. As seen in Fig. 5b and 5c, the performance of the cell with the ZnO/NDG composite-modified separator was remarkably enhanced compared with that of the cell with the normal separator. Fig. 5b presents the rate performance of the cell with and without the modified separator. The average discharge capacities of the cell with the modified separator were 902, 785, 657, and 563 mAh g^{-1} and were achieved at current densities of 0.1 C, 0.5 C, 1 C, and 2 C, respectively; these capacities were much higher than those of the cell with the pristine separator. It is worth noting that, when the C rate was returned to the initial value, the cell recovered its capacity of 842 mAh g^{-1}, and this confirms a steady cycling performance. Upon conducting the cycling test at 0.1 C (Fig. 5c), a cell with the ZnO/NDG composite-coated separator delivered a discharge capacity of 942 mAh g^{-1} for the first cycle and retained about 90.02 % of its initial discharge capacity after the 100th cycling process. However, the cell with the normal separator suffered from capacity decline and rapidly lost 26.72 % of its initial capacity after the 100th cycling test. Results suggest that the as-prepared ZnO/NDG composite can efficiently suppress the shuttling of LiPs during cycling. This result is attributed to the synergistic effect of nanosized ZnO particles and NDG; the former can chemically absorb S-related species, and the latter can act as an “upper current” collector to reuse the LiPs captured by the functional interlayer.

Preprints (www.preprints.org) | NOT PEER-REVIEWED | Posted: 30 July 2018 doi:10.20944/preprints201807.0582.v1

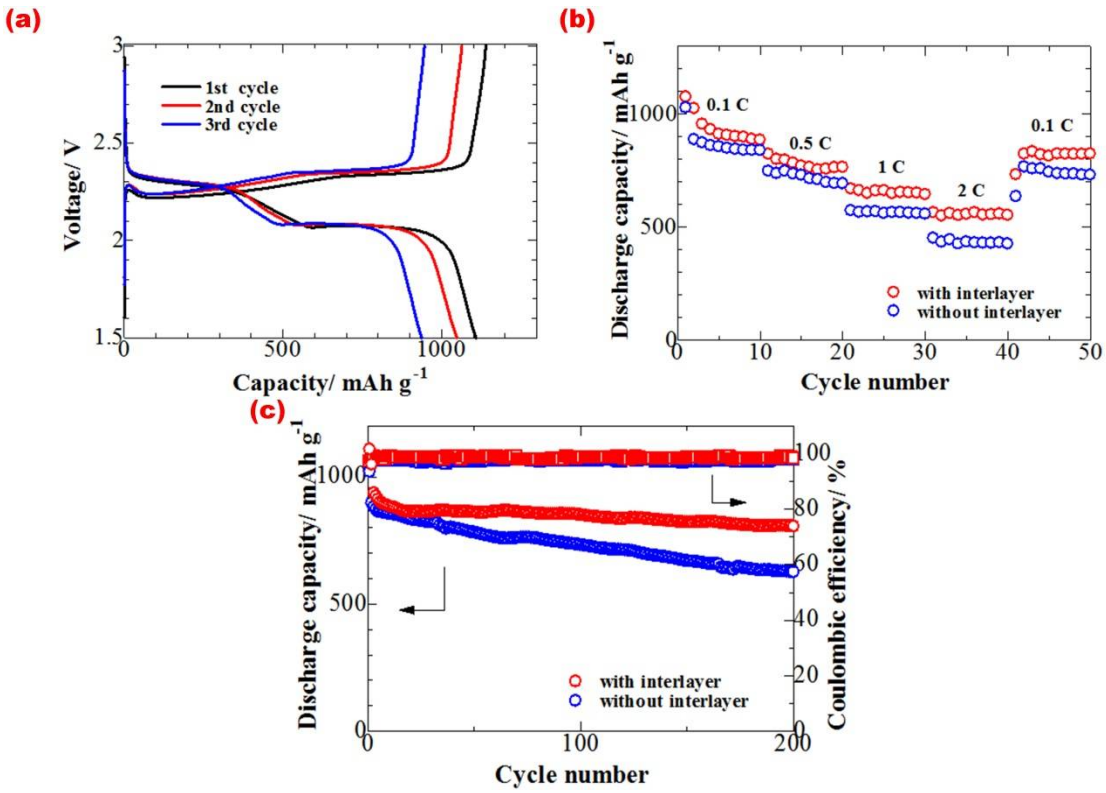

Fig. 5. Corresponding charge/discharge voltage-capacity profiles of the cell with the ZnO/NDG composite-coated separator (a). Rate performance of the cell with and without the ZnO/NDG composite-coated separator (b). Cycling performance and Coulombic efficiency of the cell with the ZnO/NDG composite-coated separator (c).

4. Conclusions

In summary, a ZnO/NDG composite was produced via a facile in situ sol-gel technique. Chemical interaction between ZnO nanoparticles and polysulfides was confirmed from XPS results after the charge/discharge cycling process. The Li/S battery benefited from the cooperation of ZnO nanoparticles and NDG, and the performance of the Li/S battery was significantly enhanced. Specifically, it delivered a high initial capacity of 942 mAh g^{-1} at 0.1 C and retained about 90.02 % of its initial discharge capacity after the 100th cycling process, and the current density performance was also evidently improved compared to the cell with the pristine separator.

Acknowledgments: The author thanks the financial of The National Natural Science Foundation of China (grant numbers 51501055, 51601056); the Natural Science Foundation of Hebei Province of China (grant number E2017202012); and the Natural Science Foundation of Shandong Province (ZR2014BL004).

Author Contributions: Data curation, gao fan; Investigation, ma ruina and du an; Methodology, tan taizhe and wen ming; Project administration, du miao and zhao xue; Resources, fan yongzhe; Writing – original draft, wang suyu; Writing – review & editing, wang suyu. **Conflicts of Interest:** The authors declare no conflict of interest.

References

1. Bruce, P.G.; Freunberger, S.A.; Hardwick, L.J.; Tarascon, J.M. Li-O-2 and Li-S batteries with high energy storage. *Nat. Mater.* **2012**, *11*, 19-29.
2. Bruce, P.G.; Hardwick, L.J.; Abraham, K.M. Lithium-air and lithium-sulfur batteries. *Mrs Bull.* **2011**, *36*, 506-512.
3. Zhang, Z.; Lai, Y.; Zhang, Z.; Li, J. A functional carbon layer-coated separator for high performance

lithium sulfur batteries. *Solid State Ionics* **2015**, *278*, 166-171.

4. Jiang, Y.; Chen, F.; Gao, Y.; Wang, Y.; Wang, S.; Gao, Q.; Jiao, Z.; Zhao, B.; Chen, Z. Inhibiting the shuttle effect of Li–S battery with a graphene oxide coating separator: Performance improvement and mechanism study. *J. Power Sources* **2017**, *342*, 929-938.
5. Evers, S.; Yim, T.; Nazar, L.F. Understanding the nature of absorption/adsorption in nanoporous polysulfide sorbents for the Li–S battery. *J. Phy. Chem. C* **2012**, *116*, 19653–19658.
6. Ji, X.; Evers, S.; Black, R.; Nazar, L.F. Stabilizing lithium-sulphur cathodes using polysulphide reservoirs. *Nat. Commun.* **2011**, *2*, 325.
7. Pang, Q.; Kundu, D.; Cuisinier, M.; Nazar, L.F. Surface-enhanced redox chemistry of polysulphides on a metallic and polar host for lithium-sulphur batteries. *Nat. Commun.* **2014**, *5*, 4759.
8. Wu, H.; Huang, Y.; Zhang, W.; Sun, X.; Yang, Y.; Wang, L.; Zong, M. Lock of sulfur with carbon black and a three-dimensional graphene@carbon nanotubes coated separator for lithium-sulfur batteries. *J. Alloy. Compd.* **2017**, *708*, 743-750.
9. Yang, X.; Ouyang, Y.; Wu, F.; Hu, Y.; Ji, Y.; Wu, Z. Size controllable preparation of gold nanoparticles loading on graphene sheets@cerium oxide nanocomposites modified gold electrode for nonenzymatic hydrogen peroxide detection. *Sensor. Actuat. B-Chem.* **2017**, *238*, 40-47.
10. Han, P.; Manthiram, A. Boron- and nitrogen- doped reduced graphene oxide coated separators for high-performance Li-S batteries. *J. Power Sources* **2017**, *369*, 87-94.
11. Li, H.; Sun, L.; Zhang, Y.; Tan, T.; Wang, G.; Bakenov, Z. Enhanced cycle performance of Li/S battery with the reduced graphene oxide/activated carbon functional interlayer. *J. Energ. Chem.* **2017**, *26*, 1276-1281.
12. Sheng-Heng, C.; Arumugam, M. High-Performance Li-S batteries with an Ultra-lightweight MWCNT-Coated Separator. *J. Phys. Chem. Lette.* **2015**, *5*, 1978.
13. Chen, G.; Song, X.; Wang, S.; Wang, Y.; Gao, T.; Ding, L.-X.; Wang, H. A multifunctional separator modified with cobalt and nitrogen co-doped porous carbon nanofibers for Li–S batteries. *J. Membrane Sci.* **2018**, *548*, 247-253.
14. Zhu, J.; Ge, Y.; Kim, D.; Lu, Y.; Chen, C.; Jiang, M.; Zhang, X. A novel separator coated by carbon for achieving exceptional high performance lithium-sulfur batteries. *Nano Energy* **2016**, *20*, 176-184.
15. Zhang, Y.; Zhao, Y.; Yermukhambetova, A.; Bakenov, Z.; Chen, P. Ternary sulfur/polyacrylonitrile/$Mg_{0.6}Ni_{0.4}O$ composite cathodes for high performance lithium/sulfur batteries. *J. Mater. Chem. A* **2012**, *1*, 295-301.
16. Song, H.; Zuo, C.; Xu, X.; Wan, Y.; Wang, L.; Zhou, D.; Chen, Z. A thin TiO_2 NTs/GO hybrid membrane applied as an interlayer for lithium–sulfur batteries. *RSC Adv.* **2018**, *8*, 429-434.
17. Shao, H.; Wang, W.; Zhang, H.; Wang, A.; Chen, X.; Huang, Y. Nano-TiO_2 decorated carbon coating on the separator to physically and chemically suppress the shuttle effect for lithium-sulfur battery. *J. Power Sources* **2018**, *378*, 537-545.
18. Wei, S.Z.; Li, W.; Cha, J.J.; Zheng, G.; Yang, Y.; Mcdowell, M.T.; Hsu, P.C.; Cui, Y. Sulphur-TiO_2 yolk-shell nanoarchitecture with internal void space for long-cycle lithium-sulphur batteries. *Nat. Commun.* **2013**, *4*, 1331.
19. Han, X.; Xu, Y.; Chen, X.; Chen, Y.-C.; Weadock, N.; Wan, J.; Zhu, H.; Liu, Y.; Li, H.; Rubloff, G., *et al.* Reactivation of dissolved polysulfides in Li–S batteries based on atomic layer deposition of Al_2O_3 in nanoporous carbon cloth. *Nano Energy* **2013**, *2*, 1197-1206.
20. Xu, Q.; Hu, G.C.; Bi, H.L.; Xiang, H.F. A trilayer carbon nanotube/Al_2O_3/polypropylene separator for lithium-sulfur batteries. *Ionics* **2014**, *21*, 981-986.

21. Liu, J.; Yuan, L.; Yuan, K.; Li, Z.; Hao, Z.; Xiang, J.; Huang, Y. SnO_2 as high-efficiency polysulfide trap in lithium-sulfur battery. *Nanoscale* **2016**, *8*.
22. Zhao, L.; Li, H.; Gao, S.; Li, M.; Xu, S.; Li, C.; Guo, W.; Qu, C.; Yang, B. MgO nanobelt-modified graphene-tantalum wire electrode for the simultaneous determination of ascorbic acid, dopamine and uric acid. *Electrochimi. Acta* **2015**, *168*, 191-198.
23. Cherian, C.T.; Sundaramurthy, J.; Reddy, M.V.; Suresh, K.P.; Mani, K.; Pliszka, D.; Sow, C.H.; Ramakrishna, S.; Chowdari, B.V. Morphologically robust $NiFe_2O_4$ nanofibers as high capacity Li-ion battery anode material. *Acs Appl. Mater. Inter.***2013**, *5*, 9957.
24. Guo-Qiang, M.A.; Wen, Z.Y.; Wang, Q.S.; Jin, J.; Xiang-Wei, W.U.; Zhang, J.C. Effects of CeO_2 Nano-crystal on electrochemical properties of Lithium/Sulfur batteries. *J. Inorg. Mater.* **2015**, *30*, 913-918.
25. Kong, Y.; Luo, J.; Jin, C.; Yuan, H.; Sheng, O.; Zhang, L.; Fang, C.; Zhang, W.; Huang, H.; Xia, Y. Enhanced sulfide chemisorption by conductive Al-doped ZnO decorated carbon nanoflakes for advanced Li–S batteries. *Nano Res.* **2017**, 1-13.
26. Li, H.; Wei, Y.; Zhang, Y.; Zhang, C.; Wang, G.; Zhao, Y.; Yin, F.; Bakenov, Z. In situ sol-gel synthesis of ultrafine ZnO nanocrystals anchored on graphene as anode material for Lithium-ion batteries. *Ceram. Int.* **2016**, *42*, 12371-12377.
27. Yin, F.; Liu, X.; Zhang, Y.; Zhao, Y.; Menbayeva, A.; Bakenov, Z.; Wang, X. Well-dispersed sulfur anchored on interconnected polypyrrole nanofiber network as high performance cathode for lithium-sulfur batteries. *Solid State Sci.* **2017**, *66*, 44-49.
28. Holloway; B.C; Kraft; Shuh; D.K; Kelly; M.A; W.D. Interpretation of x-ray photoelectron spectra of elastic amorphous carbon nitride films. *Appl. Phys. Lett.* **2000**, *74*.